J Fluoresc (2015) 25:1127–1140
DOI 10.1007/s10895-015-1603-4

ORIGINAL ARTICLE

Fluorescence Titrations of Bio-relevant Complexes with DNA: Synthesis, Structural Investigation, DNA Binding/Cleavage, Antimicrobial and Molecular Docking Studies

Thesingu Rajan Arun[1] · **Ramasamy Subramanian**[2] · **Seemon Packianathan**[1] · **Natarajan Raman**[1]

Received: 29 April 2015 / Accepted: 15 June 2015 / Published online: 7 July 2015

Abstract In the present work, we attempted to develop new metal complexes (Cu(II), Co(II), Ni(II) and Zn(II)) of the imine ligand which was synthesized from 9,10-phenanthrenequinone and *para*-anisidine. With an intention to make the complexes most stable, very special chelating amino acid has been coordinated to the metal centre. The resultant metal complexes have been characterized by variety of techniques including FT-IR, UV–Vis., ^{1}H NMR, ^{13}C NMR, powder XRD, EPR and mass spectral studies. The interaction of the complexes with DNA has been effectively examined and explored by fluorescence titration, UV–Vis absorption, viscometer titration, cyclic voltammetry (CV) and differential pulse voltammetry. Moreover, molecular docking analysis has been performed to understand the nature of binding of the complexes with DNA. These studies prove that CT DNA interaction of the complexes follows intercalation mode. The metal complexes exhibit effective cleavage of pUC19 DNA by an oxidative cleavage mechanism. The antimicrobial screening indicates that these complexes are good antimicrobial agents against various organisms.

Keywords Schiff base · DNA binding · Fluorescence · DNA cleavage · Anti-pathogenic · Molecular docking

Electronic supplementary material The online version of this article (doi:10.1007/s10895-015-1603-4) contains supplementary material, which is available to authorized users.

✉ Natarajan Raman
ramchem1964@gmail.com

[1] Research Department of Chemistry, VHNSN College, Virudhunagar, Tamilnadu 626 001, India

[2] Centre for Scientific and Applied Research, PSN College of Engineering and Technology, Tirunelveli, Tamilnadu 627152, India

Introduction

Schiff base ligands (imine ligands) are being considered as the most privileged ligands in coordination chemistry owing to their capability to coordinate with different metal ions and stabilize the metal center in multiple oxidation states [1]. If the additional functional groups present in Schiff base ligand, the stability of metal complexes will be enhanced through chelation [2]. Along with these characteristics, the widespread application of Schiff bases in various fields including optics, sensors and pharmaceutics make them, very attractive. After metallation with transition metal ions, the applications of Schiff base ligands have been proved to be effectively mounted and extended [3]. As a result, transition metal complexes of Schiff base ligands are reported as the potential candidates in modern research as oxygen carriers [4], metalloenzymes [5], catalysts [6] and sensors [7]. Prominently, their action against diabetes, bacteria, fungi, and tumor is remarkable and being fascinated till now [8, 9]. To establish a metal complex as a new drug, its stability under different metabolic conditions is a serious issue. Amino acids can act as typical ligands to stabilize the metal complexes by chelating the metal ions via amino (NH_2) and carboxylate (COO^-) functional groups [10]. Coordination of amino acid ligands to the vacant coordination sites of Schiff base complexes not only increases the stability but also results in the incredible biological properties. Moreover, connecting amino acids with metal ions may produce the model systems to study the metal–metal interactions of metalloproteins [11]. Among the studied amino acid ligands, histidine is very attractive because its imidazole functional group can do wonders during the action of metalloenzymes [12]. Current research suggests that histidine can act as a neuroprotective [13] and natural detoxifier which protects radiation hazards and removes heavy metals from the environment. Further, histidine may

even help to prevent the onset of AIDS and it is crucial for the production of both red and white blood cells. Thus in the present study, histidine has been incorporated into the Schiff base complex through the vacant coordination sites of metal centre with the motive to reach an innovative metal complex.

DNA executes an imperative constituent for many biochemical progressions that arise in the cellular system. The dissimilar sequences present in the DNA are implicated in various regulatory processes such as gene expression, gene transcription, mutagenesis, carcinogenesis etc [14]. The above mentioned processes can be modified by the interaction of chemical compounds with specific regions of DNA. This smash may lead to a variety of pathological changes in living organisms. It has been proven that growth of tumor cells can be inhibited by altering the DNA replication of tumor cells. Thereby interaction between DNA and chemical molecules gets fired in the midst of biochemists. Schiff base metal complexes have shown to be the vital anti-cancer agents due to their binding with DNA. Therefore over a decade, there has been an incessant interest in the interaction of Schiff base metal complexes with DNA. Metal complexes can bind DNA by non-covalent interactions such as electrostatic binding, groove binding and intercalative binding [15]. Intercalative binding mode has been reported more effective than other binding modes. Intercalators are small molecules which have a planar aromatic heterocyclic functionality, able to stack between the base pairs of double helical DNA [16].

By considering the above facts in our mind, herein we reported the new Schiff base metal complexes having histidine as the ancillary ligand in its vacant coordination sites. They have been synthesized and characterized by variety of techniques including UV–Vis., FT-IR, ^{1}H NMR, ^{13}C NMR, powder XRD, mass. The DNA binding was explored by fluorescence titration, UV–Vis absorption, viscometer titration, cyclic voltammetry (CV) and differential pulse voltammetry.

Experimental

Materials

All reagents were of best commercial grade and were used without further purification. 9,10-phenanthrenequinone, *para*-anisidine, histidine (His) and Ethidium bromide (EB) were obtained from Sigma Aldrich. Calf thymus DNA (CT DNA) (Himedia, India) and pUC19 plasmid DNA (Bangalore Genei, India) were used for DNA binding and DNA cleavage studies. All other chemicals, solvents and metal salts were procured from E-Merck, India.

Physical Measurements

Elemental analysis (C, H and N) data were obtained using a Perkin-Elmer 240 elemental analyzer. Vibration spectra were performed on FTIR–Shimadzu model IR-Affinity-1 spectrophotometer using KBr discs. The NMR spectra of the ligand and Zn(II) complex were recorded on a Bruker Advance DRX 300 spectrometer operating at room temperature (RT). RT magnetic susceptibility measurements were carried out on a modified Gouy-type magnetic balance, Hertz SG8-5HJ. The molar conductivity of the complexes in DMSO solution (10^{-3} M) was measured in a deep vision 601 model digital conductometer at RT. Powder X-ray diffraction (powder-XRD) measurements were done on an X-ray diffractometer (XPERT-PRO PANALYTICAL) for phase identification between 2θ range, 10–80°. The X-band EPR spectrum was accomplished at liquid N_2 temperature (77 K) using tetracyanoethylene (TCNE) as the g-marker. Shimadzu Model 1601 UV–Visible spectrophotometer and Hitachi F–2500 fluorescence spectrophotometer were employed to attain the electronic and fluorescence spectra, respectively. Cyclic voltammetric (CV) experiments were achieved on a CHI 620C electrochemical analyzer in freshly distilled DMSO solution.

Synthesis of Schiff Base (L)

For the synthesis of L, 1 mmol 9,10-phenanthrenequinine and 2 mmol *p*-anisidine were taken in ethanol. To this ethanolic solution, few drops of glacial acetic acid were added and refluxed for 4 h. The solid product formed was filtered, washed, dried and recrystallized from ethanol, dried in vacuo.

[*L*] *Yield*: 71 %; yellow colour; Anal.Calc. (%): C (80.3), H (5.3) and N (6.6); Found (%): C (80.1), H (5.1) and N (6.3); FT-IR (KBr) (cm^{-1}): 1629(−C=N), 2900–2950 (C-H) and 1400–1600 (C=C); ^{1}H NMR (DMSO-d_6) δppm: (Ar-H) 6.5–7.6 (m), (O-CH_3) 3.6–3.7(s); ^{13}C NMR (DMSOd_6): δppm 124.0–136.2 (Ar-C), 54.3 (O-CH_3), 153.4 (−C=N); UV–Vis. In DMSO, nm (transition): 268 (π-π*) and 376 (n-π*).

Synthesis of Metal Complexes

To synthesize metal complexes, primarily L (0.01 M) and the metal chloride salt (0.01 M) were mixed in a portion of ethanol (40 mL). This mixture was then stirred at ambient temperature for 4 h. Histidine (0.02 M) in 1:1 water-ethanol mixture was added to the above mixture and allowed to reflux for 6 h. The resultant product was washed with ethanol and then recrystallized. The obtained solid product was filtered, dried in vacuo at 60 °C and kept in desiccator.

[$CuL(His)_2$]: Yield: 67 %; brown colour; Anal.Calc.(%): C (61.2), H (5.0), N (13.9) and Cu (7.9); Found (%): C (60.8), H

(4.7), N (13.4) and Cu (7.6); FT-IR (KBr) (cm^{-1}): 1622 (−C=N), 3242 (NH_2), 1476 ($\upsilon_{asy}(COO^-)$), 1386 ($\upsilon_{sy}(COO^-)$), 526 (M-O) and 437 (M-N); Λ_m (Ω^{-1} mol^{-1} cm^2) 15.2; μ_{eff} (BM) 1.83; UV–Vis. in DMSO, nm (transition): 430 (LMCT) and 916 (d-d).

[*CoL*(*His*)$_2$]: Yield: 71 %; green colour; Anal.Calc (%): C (61.5), H (5.0), N (14.1) and Co (7.3); Found (%): C (61.2), H (4.7), N (13.8) and Co (7.1); FT-IR (KBr) (cm^1): 1618 (−C=N), 3160 (NH_2), 1440 ($\upsilon_{asy}(COO^-)$), 1390 ($\upsilon_{sy}(COO^-)$), 532 (M-O) and 439 (M-N); Λ_m (Ω^{-1} mol^{-1} cm^2) 20.3; μ_{eff} (BM) 4.86; UV–Vis. in DMSO, nm (transition): 429 (LMCT) and 907 (d-d).

[*NiL*(*His*)$_2$]: Yield: 64 %; yellow colour; Anal.Calc (%): C (61.5), H (5.0), N (14.0) and Ni (7.3); Found (%): C (61.2), H (4.7), N (13.8) and Ni (7.1); FT-IR (KBr) (cm^{-1}) 1614 (−C=N), 3234 (NH_2), 1443 (υ_{asy}(COO)), 1376 (υ_{sy}(COO)), 527 (M-O) and 437 (M-N); Λ_m (Ω^{-1} mol^{-1} cm^2) 21.6; μ_{eff} (BM) 3.18; UV–Vis. in DMSO, nm (transition): 388 (LMCT) and 906 (d-d).

[*ZnL*(*His*)$_2$]: Yield: 68 %; greenish yellow colour; Anal.Calc (%) C (61.0), H (5.0); N (13.9) and Zn (8.1); Found (%): C (60.6), H (4.6), N (13.6) and Zn (7.8); FT-IR (KBr) (cm^{-1}): 1608 (−C=N), 3261 (NH_2), 1448 ($\upsilon_{asy}(COO^-)$), 1375 ($\upsilon_{sy}(COO^-)$), 529 (M-O) and 438 (M-N); ^{1}H NMR (DMSO-d_6) δppm: (Ar-H) 6.4–7.6 (m), (−NH_2) 4.4 (s), (O-CH_3) 3.6–3.7(s), 1.2–1.6 (C−H) (His-H); ^{13}C NMR (DMSO-d_6) δppm: 124.0–136.2 (Ar-C), 150.1 (−C=N), 54.1–54.3 (O-CH_3) and 180.4 (COO^-); Λ_m (Ω^{-1} mol^{-1} cm^2) 18.4; μ_{eff} (BM) diamagnetic; UV–Vis. in DMSO, nm (transition): 394 (LMCT).

DNA Binding Experiments

All of the experiments involving the binding of complexes with CT DNA were carried out in double distilled water with Tris–HCl [(hydroxymethyl) aminomethane] (Tris–HCl, 5 mM) and NaCl (50 mM) and adjusted to pH 7.2 with hydrochloric acid. A solution of CT DNA in the buffer gave a ratio of UV absorbance of about 1.89:1 at 260 and 280 nm, indicating that the DNA was sufficiently free of protein [2].

Electronic Absorption Spectroscopy Experiments

Absorption titration experiments were performed by maintaining a constant concentration of the complexes (30 μL), but varying the CT DNA concentration (0–180 μL) in buffer. After each addition of CT DNA to the complexes, the absorption readings were noted. The data were then fitted to the following Eq. (1) to obtain the intrinsic binding constant K_b values for interaction of the complexes with DNA.

$$[DNA]/(\varepsilon_a-\varepsilon_f) = [DNA]/(\varepsilon_b-\varepsilon_f) + 1/[K_b((\varepsilon_b-\varepsilon_f)] \quad (1)$$

In the above equation, [DNA] denotes the concentration of DNA, absorption coefficients ε_a, ε_f and ε_b correspond to A_{obs}/[complex], free complex′s extinction coefficient and the extinction coefficient of the complex in the totally bound form, respectively. From the equation (Eq. (1)), slope ($1/(\varepsilon_b - \varepsilon_f)$) and intercept ($1/[K_b(\varepsilon_b - \varepsilon_f)]$) were found out. Finally by comparing the identified slope and intercept, K_b was calculated.

Fluorescence Spectroscopy Experiments

DNA was pre-treated with ethidium bromide in the ratio [DNA] = 10 μL, [EB] = 5 μL for 30 min at 27 °C. EB was non-emissive in Tris–HCl buffer solution (pH 7.2) due to fluorescence quenching of the free EB by the solvent molecules. In the presence of DNA, EtBr showed enhanced emission intensity due to its intercalative binding to DNA. The excitation wavelength 370 nm was fixed for EtBr bound to DNA. The change in intensity was recorded with an increasing amount of the metal complexes (30–150 μL), added to this mixture and their effect on the emission intensity was measured [17]. According to the Stern-Volmer equation:

$$I_0/I = Ksv[Q] + 1$$

where, I_0 is the emission intensity in the absence of a quencher, I is the emission intensity in the presence of a quencher, Ksv is the Stern- Volmer quenching constant, and [Q] is the quencher concentration. The Ksv quenching constant value is obtained as a slope from the plot of I_0/I versus [Q].

Cyclic Voltammetric Experiments

With the motive to do DNA binding studies of the complexes, a three electrode system [working electrode (glassy carbon), auxiliary electrode (platinum wire) and reference electrode (Ag/AgCl)] was set in CHI620C electrochemical analyzer to carry out cyclic voltammetric and differential pulse voltammetric studies. All the solutions prepared for the study were degassed by purging N_2. All the electrodes were cautiously rinsed with de-ionized water prior to the proceedings.

The degree of reversibility of one electron transfer reaction can be received from the difference between forward and backward peak potentials. The ratio of equilibrium constants for the binding of oxidative and reductive ions to DNA was calculated by the Nernst equation as given in Eq. (2).

$$E_b - E_f = 0.0591 \log \left(K_{[red]}/K_{[oxd]}\right) \quad (2)$$

where E_b^o and E_f^o are the potentials of the bound and free complex forms, respectively; K_{red} is the binding constant for the binding of reductive ion species with CT DNA and K_{oxd} is the binding constant for the binding of oxidative ion species with CT DNA.

Viscosity Experiments

The DNA solution of a viscosity has been measured at room temperature in the presence of increasing amounts of the complexes upto r value of 0.35. The acquired data are presented as $(\eta/\eta_0)^{1/3}$ and the ratio of the concentration of the complexes to CT DNA, where η is the viscosity of DNA in the presence of compound, and η_0 is the viscosity of DNA alone in buffer solution.

Chemical Nucleus Activity

The ability of L and transition metal complexes to cleave pUC19 DNA was studied by gel electrophoresis. To accomplish the DNA cleavage reactions, the solutions of pUC19 DNA were prepared afterward diluted with loading dye using 1 % agarose gel. To the above solution, 3 μM of ethidium bromide was added and mixed well. In the next step, the warm agarose was transferred and instantly hold tightly with a comb to develop sample wells. In electrophoresis tank, the gel was placed and adequate electrophoretic buffers were added to enclose the gel to 1 mm depth. DNA sample (20 μM), complexes (30 μM) and H_2O_2 (500 μM) in the aforesaid buffer (pH 7.2) were mixed with a loading dye and full into the well of the submerged gel using a micropipette. The 50 mA electric current was passed and the gel was taken out from the buffer. The gel was viewed in an UVITEC Cambridge Gel doc system and photographed using a CCD camera.

Antimicrobial Screening

The in vitro antimicrobial bustle of the L and its corresponding complexes have been carried out against certain human sensitive pathogenic Gram-positive bacteria (*Staphylococcus aureus* and *Nocardia asteroides*) and Gram-negative bacteria (*Klebsiella pneumoniae* and *Escherichia coli*) and fungi (*Aspergillus niger*, *Fusarium solani* and *Candida albicans*) using dilution method [18]. The nutrient agar and dextrose agar were served as the medium for the growth of bacteria and fungi, ciprofloxacin and fluconazole were chosen as standards for antibacterial and antifungal activity, respectively. The samples were incubated at 37 °C for 24 h (bacteria) and 48 h (fungi), respectively. The results were recorded in terms of MIC (the lowest concentration of test substance which inhibited the growth of microorganisms).

Software Details

Computational studies of L and metal complexes have been performed using HEX 6.3 software which is an interactive molecular graphics program for the interaction, docking calculations, and to identify possible binding site of the biomolecules. The crystal structure of B-DNA (PDB ID: 1BNA) is downloaded from the protein data bank. All possible poses have been considered as starting points and the docking analysis was performed.

Results and Discussion

Synthetic Route and General Properties of $[ML(His)_2]$

The general synthetic pathway for the heterocyclic imine ligand (L) and the mixed ligand metal complexes is represented in Scheme 1. Both L and derived complexes are found to be air stable over the extended periods. L is dissolved in common organic solvents whereas metal complexes are only soluble in DMSO and DMF. The very similarity between the obtained elemental analysis data of L and the complexes suggests the stoichiometry, $[ML(His)_2]$. The DMSO solution of the metal

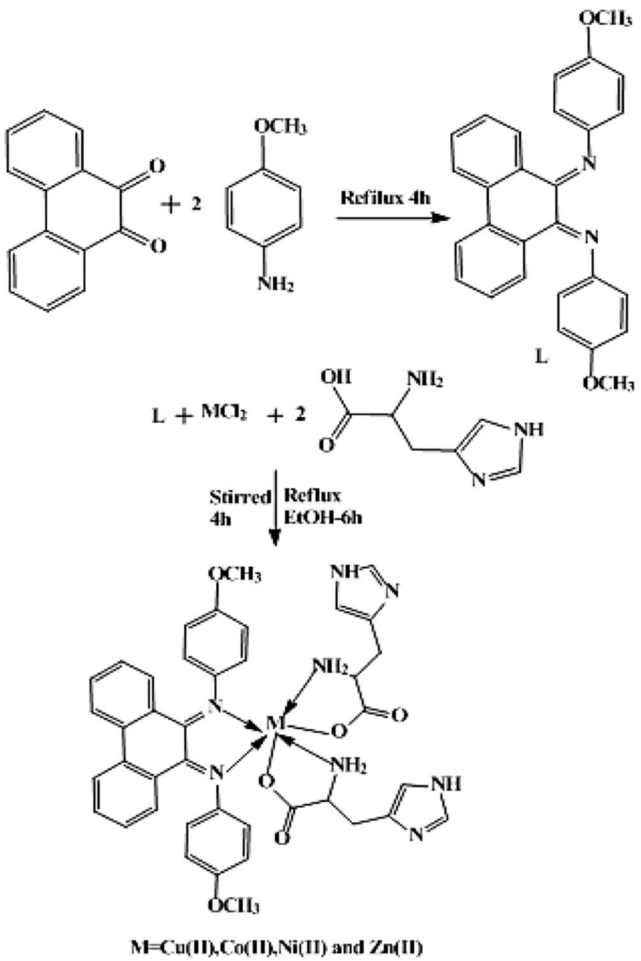

Scheme 1 Schematic route for the synthesis of imine(−C=N) ligand (L) and its mixed ligand metal complexes

complexes shows lower molar conductance values (15.2–21.6 ohm^{-1} cm^2 mol^{-1}) which might be due to the non-electrolytic nature of the complexes.

IR Spectra

Vibrational spectroscopy is the best method to find out the functional groups available in the chemical compounds. It has been also utilized to scrutinize the coordination reaction between the metal ions and the donor sites of ligands. The FT-IR spectra of L and the complexes are given in Fig. 1. In Fig. 1a, the emergence of peak at 1629 cm^{-1} is attributed to the characteristic peak of imine functional group which supports the formation of L from 9,10-phenanthrenequinone and *para*-anisidine. The bands observed in the region of 1400–1600 cm^{-1} are due to the aromatic C=C bonds. The peaks at around 3000 cm^{-1} are appeared because C-H bonds present in aromatic rings. The presence of –OCH_3 in L is affirmed by the C-H stretching frequencies noted at 2850 cm^{-1}. FT-IR spectra of the complexes show the similar spectral pattern to L except few significant changes. Notably, the lower region shift in the distinctive peak of imine functional group is assigned to the coordination of imine nitrogen to metal centre of the complexes. This observation is further supported by M-N characteristic peak noted at ~435–451 cm^{-1} in all the complexes. The coordination of histidine to the metal centre can be confirmed by the existence of characteristic –NH_2 peak in all the complexes. As expected, such –NH_2 peak is appeared as the continuing band in all the complexes between the region 3000–3270 cm^{-1} and it signifies the incorporation of histidine to the synthesized complexes [19]. Furthermore, the bands appeared at ~1470 and ~1385 cm^{-1} which are assigned to asymmetric and symmetric stretches of carboxylato anion [20] (COO^-) of histidine moiety, also confirm the coordination of histidine to the metal centre. This can be again proved by the characteristic M-O stretches at ~530 cm^{-1}. Thus FT-IR spectral studies assure the formation of L and the complexes which have histidine as the secondary ligand.

Electronic Spectra

The UV–Vis spectra of both L and the complexes are represented in supplementary file (Fig. S1). In the UV spectrum of ligand, two characteristic absorption bands are found. A weak absorption band at 268 nm is due to the π-π* transition of π electrons present in aromatic ring (C=C) and imine group (−C=N). The strong absorption band at 376 nm is allocated to n-π* transition of non-bonded electrons available in imine group. UV spectra of the complexes also exhibit these characteristic n-π* and π-π* transitions however they slightly differ either in position or intensity, which may be the result of coordination of L with metal centre. Ligand to metal charge transfer (LMCT) transition can also be identified around 430 nm in UV spectra of all the complexes [21]. Besides, metal complexes reveal an extra and much significant characteristic band that appears as the result of d-d transition. This d-d transition is very useful to predict the geometry of the metal complexes. The electronic spectrum of [$CuL(His)_2$] shows its d–d transition band at 916 nm which is the sign of $^2E_g \rightarrow {}^2T_{2g}$ transition. This d-d transition suggests distorted octahedral geometry to [$CuL(His)_2$] complex [22]. [$CoL(His)_2$] shows

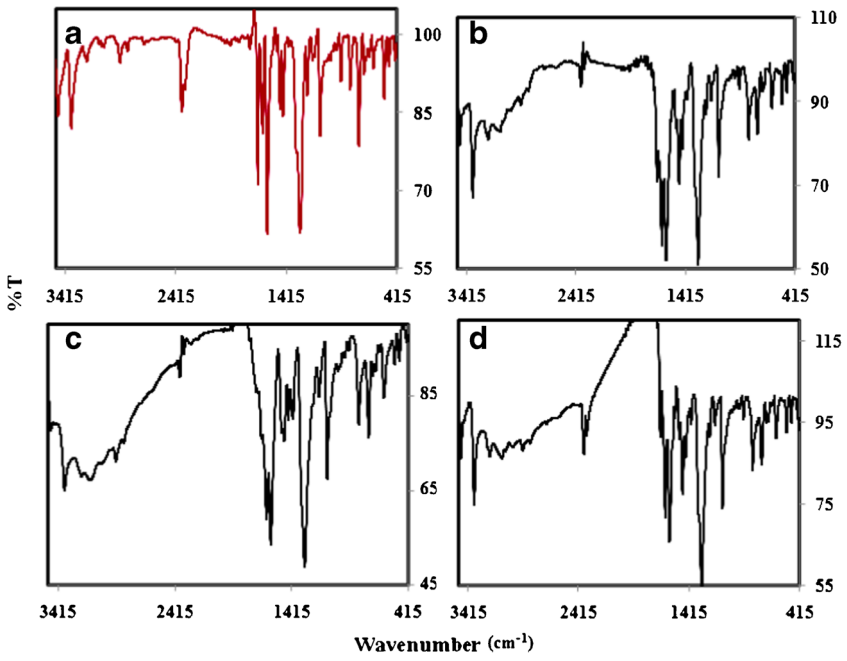

Fig. 1 FT-IR spectra of **a** L **b** [$CuL(His)_2$], **c** [$NiL(His)_2$] and **d** [$ZnL(His)_2$]

this d-d transition $^4T_{1g}(F) \rightarrow {}^4T_{2g}(F)$ at 907 nm as the result of octahedral geometry. In the UV–Vis spectrum of $[NiL(His)_2]$, the bands observed at 1088 and 906 nm are assigned to the electronic transitions $^3A_{2g}(F) \rightarrow {}^3T_{2g}(F)$, and $^3A_{2g}(F) \rightarrow {}^3T_{1g}(F)$, respectively, and suggest the octahedral geometry to $[NiL(His)_2]$ [23].

^{1}H NMR and ^{13}C NMR Spectra

The ^{1}H NMR spectra of L and diamagnetic $[ZnL(His)_2]$ have been recorded in DMSO-d_6 using TMS as the internal standard. The ^{1}H NMR spectrum of L exhibits multiplet at 6.59–7.69 ppm which is the characteristic of the protons of aromatic phenyl rings. Moreover, the L exhibits singlet at 3.6–3.7 ppm which is the characteristic of methoxy proton ($-OCH_3$). However in the ^{1}H NMR spectrum of $[ZnL(His)_2]$, an additional peak gets evolved between 1.23–1.61 ppm and it could be due to histidine proton moiety (C−H). The ^{1}H NMR peaks of $-NH_2$ protons of amino acid are normally expected to be present at 5.1 ppm, but herein $[ZnL(His)_2]$, it is shifted to downfield region (4.4 ppm). It proves the clear indicative of histidine's involvement in coordination with Zn(II). On comparison with ^{1}H NMR spectrum of L, there is no noticeable change in the aromatic proton signals of $[ZnL(His)_2]$. The ^{13}C NMR spectrum of L exhibits aromatic carbon signals between 124.0–136.2 ppm. It also exhibits the other important peaks at 153.4 and 53.4 ppm, characteristic of -C=N and methoxy ($-OCH_3$) bond. In the case of $[ZnL(His)_2]$, such distinctive peak of -C=N bond gets shifted to 150.1 ppm and a new peak is also seen at 180.42 due to the COO^- group. This evidence of COO^- group greatly supports the coordination of histidine with Zn(II) metal centre.

Powder-XRD

The obtained XRD diffractograms of $[CuL(His)_2]$ and $[CoL(His)_2]$ are presented in Fig. 2. Both the complexes display sharp crystalline peaks and it indicates their crystalline nature. On the other hand, such crystalline peaks are not resolved in the XRD analysis of $[NiL(His)_2]$ and $[ZnL(His)_2]$ which suggests amorphous nature to them [24]. The X–ray diffractogram of $[CuL(His)_2]$ shows the reflecting peaks at 2θ of 19.29°, 23.22°, 25.56°, 26.55°, 28.44°, and 29.57° and they are assigned to (201) (020), (202), (220), (102) and (401), respectively. These assignments effectively propose the orthorhombic crystal structure of $[CuL(His)_2]$ (JCPDF: No.71–0129) [25]. Likewise XRD pattern of $[CoL(His)_2]$ exposes reflecting peaks at 2θ of 22.37°, 26.47° and 44.86° due to (104), (007) and (117) crystal planes, respectively. It also reveals the orthorhombic structure of Co(II) atoms (JCPDF No. 27-1029). The grain sizes of the complexes can be predictable

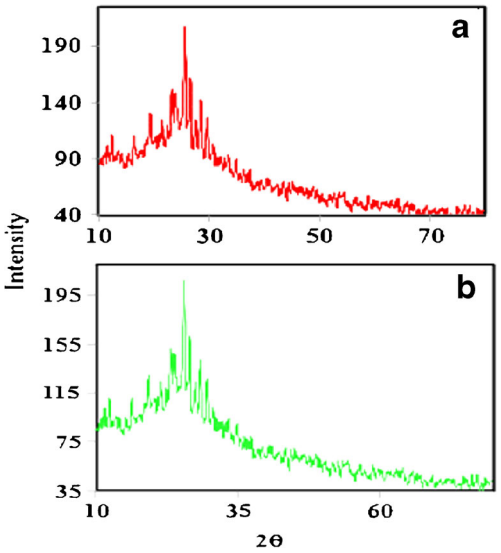

Fig. 2 Powder XRD patterns of **a** $[CuL(His)_2]$ and **b** $[CoL(His)_2]$

from the main XRD peak by using the Scherer's equation [26] as follows:

$$D = 0.9\lambda/\beta\cos\theta$$

where λ is the wavelength of the X-ray radiation (λ = 0.15406 nm), β is the full width half maximum of the characteristic peak (in radians) corrected for instrumental broadening, θ is Bragg diffraction angle for hkl plane and D is the grain size (nm). Experiential average grain sizes of the $[CuL(His)_2]$ and $[CoL(His)_2]$ complexes are established to be 45 and 35 nm, respectively.

EPR Spectrum of $[CuL(His)_2]$

EPR spectroscopy has been recognized as the conventional technique to explore the geometry of metal complexes and bonding parameters, in particular copper complexes [27]. In the present study, EPR spectrum of $[CuL(His)_2]$ was performed. The recorded EPR spectrum of $[CuL(His)_2]$ is illustrated in supplementary file (Fig. S2). The calculated spin Hamiltonian spectral parameters of $[CuL(His)_2]$ are listed in supplementary file (Table S1). The $g_{||}$, $g_{\perp}$ and g_{iso} values were calculated from the spectra using tetracyanoethylene (TCNE) free radical as 'g' marker. These g values are effectively involved in determining the axial symmetry parameter (G) using the following equation:

$$G = \left(g_{||} - 2\right)/\left(g_{\perp} - 2\right)$$

If G > 4.0, the local tetragonal axes are considered to be aligned parallel or slightly misaligned. If G < 4.0, significant exchange coupling might be present and the considerable misaligned will be there. In our case, G value for $[CuL(His)_2]$ is 4.56 which means that the local tetragonal axes

are aligned parallel or slightly misaligned and the unpaired electron is present in the d_x^2-$_y^2$ orbital. The lesser value of $g_{||}$ (2.25) as compared to 2.3 is a good evidence for the covalent character of metal–ligand interactions [28]. The observed $g_{||}/A_{||}$ value for the $[CuL(His)_2]$ is 163 and specifies the distorted octahedral geometry of $[CuL(His)_2]$. This EPR investigation greatly supports the results acquired from UV–Vis. spectroscopy.

EPR bonding parameters (α^2, β^2 and γ^2) of $[CuL(His)_2]$ have been calculated and summarized in supplementary file (Table S2). The bonding parameters α^2, β^2 and γ^2 are regarded as the measure of covalence of the in-plane σ-bonds, in-plane π-bonds and out of plane π-bonds, respectively. α^2 can be calculated using the equation,

$$\alpha^2 = \left(A_{||}/0.036\right) + \left(g_{||}-2.0023\right) + 3/7\left(g_{\perp}-2.0023\right) + 0.04$$

For pure covalent bonding, $\alpha^2 = 0.5$ while it equals to 1.0 for pure ionic bonding. In the present case, α^2 value is 0.6178 for $[CuL(His)_2]$ which designates that the complex has some covalent character. The in plane π-bonding (β^2) and out of plane π bonding (γ^2) parameters are calculated from the following equations:

$$\beta^2 = \left(g_{||}-2.0023\right)E/\left(-8\lambda\alpha^2\right)$$
$$\gamma^2 = \left(g_{\perp}-2.0023\right)E/\left(-2\lambda\alpha^2\right)$$

where $\lambda = -828$ cm-^{1} for free Cu(II) ion and E (916 nm) is the electronic transition energy of $[CuL(His)_2]$. The observed values of β^2, γ^2 for $[CuL(His)_2]$ are 0.6234 and 0.5182, respectively. It apparently shows that β^2 is greater than γ^2. It may be due to the interaction in out of plane π-bonding. These can be also proved by the values of $K_{||}$ and $K_{\perp}$ ($K_{||}$ and $K_{\perp}$ are the parallel and perpendicular components of the orbital reduction factor (K), respectively). Hathaway [29], pointed out that for pure σ-bonding, $K_{||} \approx K_{\perp} = 0.77$ and for in-plane π -bonding $K_{||} < K_{\perp}$, while for out of plane π-bonding, $K_{\perp} < K_{||}$. The following simplified expressions were used to calculate $K_{||}$ and $K_{\perp}$,

$$K_{||} = \left[\left(g_{||}-2.0023\right)DE\right]/8\lambda_o$$
$$K = \left[(g-2.0023)DE\right] / 8\,\lambda_o$$

where λ_o is the spin orbit coupling constant for the Cu(II) ion (–828 cm^{-1}). The observed $K_{||}$ (0.6246) and $K_{\perp}$ (0.1177) values imply a greater contribution of out-of-plane π-bonding than in-plane π-bonding in metal-ligand π-bonding.

Mass Spectra

The mass spectra of the imine ligand (L) and its $[CuL(His)_2]$ are given in supplementry file (Fig. S3). The mass spectrum of imine ligand (L) showed molecular ion peak at m/z = 388 [M$^+$] corresponding to $[C_{27}H_{19}N_2O]^+$ ion. Also the spectrum exhibits peaks for the fragments at m/z 419, 357, 298, 122, 107 and 91 corresponding to $[C_{28}H_{22}N_2O_2]^+$, $[C_{26}H_{16}N_2]^+$, $[C_{21}H_{15}NO]^+$, $[C_7H_7NO]^+$, $[C_7H_7O]^+$ and $[C_7H_6]^+$ respectively (Fig. S3a). Moreover, the mass spectra of $[CuL(His)_2]$ complex showed peaks with m/z 388 (Base peak), 805, 496, 419, 384, 357, 298, 153, 122, 107 and 91 corresponding to $[C_{27}H_{19}N_2O]^+$, $[C_{41}H_{40}N_8O_6Cu]^+$, $[C_{29}H_{24}N_2O_2Cu]^+$, $[C_{28}H_{22}N_2O_2]^+$, $[C_{13}H_{18}N_6O_4Cu]^+$, $[C_{26}H_{16}N_2]^+$, $[C_{21}H_{15}NO]^+$, $[C_6H_8N_3O_2]^+$, $[C_7H_7NO]^+$, $[C_7H_7O]^+$ and $[C_7H_6]^+$ respectively (Fig. S3b). The m/z of all the fragments of Schiff base ligand and its metal complex confirm the stoichiometry of the complexes of the type $[ML(His)_2]$. The mass spectra of ligand (L) and its complexes show molecular ion peaks which are in good agreement with the structure suggested by elemental analysis, magnetic and spectral studies.

DNA Binding Studies

DNA is the primary pharmacological target for antitumor drugs and therefore, to establish a new drug, it is crucial to investigate its binding ability with DNA [30]. Herein also, the DNA binding ability of $[ML(His)_2]$ (M=Cu/Co/Ni/Zn) has been explored. In such attempt, we employed many analytical techniques including UV–Vis., fluorescence, viscosity and electrochemical. From the set of investigations, the mode of binding between DNA and $[ML(His)_2]$ has been found out.

Electronic Absorption Titration

Electronic absorption spectroscopy is one of the most effective methods to ascertain the binding mode of $[ML(His)_2]$ with CT DNA and binding constants (K_b) [31]. It is universally accepted that the small molecules which interact with CT DNA via intercalation are typically resulted in the absorbance changes as well as wavelength shifts due to their binding with DNA. The absorption spectra of $[ML(His)_2]$ in the absence and presence of CT DNA are depicted in Fig. 3. Hypochromic and bathochromic shifts are noted upon increasing DNA concentration with constant concentration of $[ML(His)_2]$. The % of observed hypochromisms are 10.4, 6.3, 7.5 and 7.1 % for $[CuL(His)_2]$ (380 nm), $[CoL(His)_2]$ (381 nm), $[NiL(His)_2]$ (377 nm) and $[ZnL(His)_2]$ (380 nm), respectively. These bands are appeared due to the intra-ligand π–π* transition available in the corresponding complexes. These considerable hypochromic and bathochromic shifts might be due to the intercalative mode of DNA binding which may occur by the strong stacking between the aromatic chromophore of $[ML(His)_2]$ and the base pairs of DNA [32]. In order to compare the CT DNA-binding affinity of the studied complexes quantitatively, their intrinsic binding constants were calculated

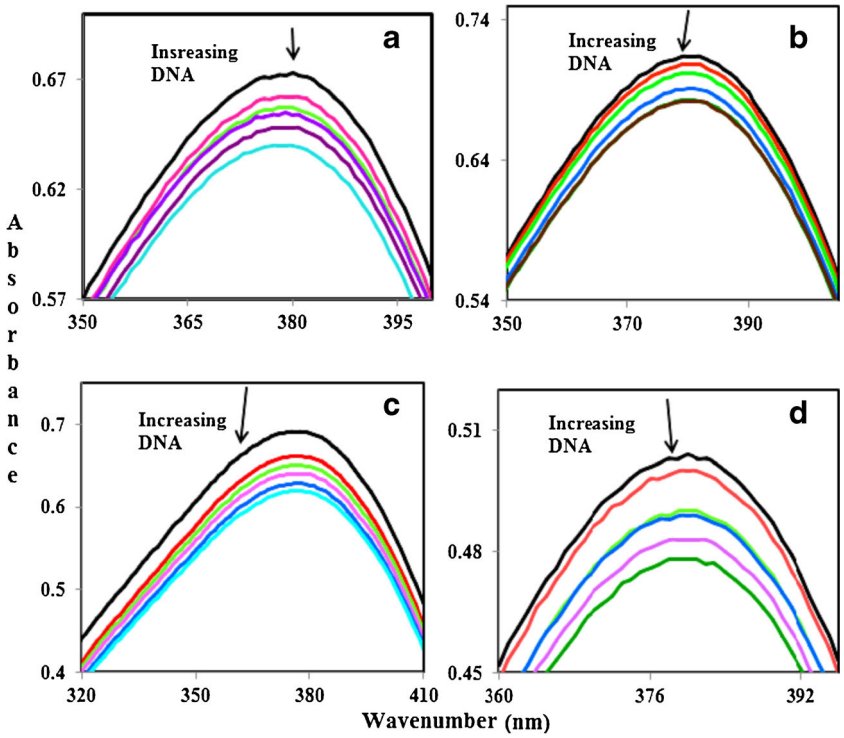

Fig. 3 Absorption spectra of **a** $[CuL(His)_2]$, **b** $[CoL(His)_2]$, **c** $[NiL(His)_2]$ and **d** $[ZnL(His)_2]$ complexes in buffer pH = 7.2 at 25 °C in presence of increasing amount of DNA. *Arrow* indicates the changes in absorbance upon increasing the DNA concentration

by the changes associated with LMCT absorption upon increasing the concentrations of CT DNA. The calculated values are given in Table 1. The determined intrinsic binding constants for $[CuL(His)_2]$, $[CoL(His)_2]$, $[NiL(His)_2]$ and $[ZnL(His)_2]$ are $5.8 \times 10^5\ M^{-1}$, $1.4 \times 10^5\ M^{-1}$, $2.8 \times 10^5\ M^{-1}$ and $3.7 \times 10^5\ M^{-1}$, respectively. Hence, it shows that the observed K_b value of the present complexes is lower than that for a classical intercaltor, such as EB and higher than those of some metal complexes [17] indicating that the present complexes strongly bind with DNA through an intercalation mode at the double helix structure of DNA.

Fluorescence Titration

In order to further confirm the intercalating mode of binding, fluorescence titration has been accomplished with EB-DNA system [33]. EB is non-emissive in Tris–HCl buffer solution (pH 7.2) due to fluorescence quenching of free EB by the solvent molecules. It is already reported that EB can show enhanced emission intensity in presence of DNA, due to its strong intercalation between the adjacent DNA base pairs [34]. The mode of interaction between the studied complexes and DNA was assessed by the EB–DNA compound system. The EB-DNA is helpful based on the basis of decrease of fluorescence as the result of EB displacement from a DNA sequence by a quencher. The fluorescence spectra of EB–DNA system quenched by $[CuL(His)_2]$ and $[ZnL(His)_2]$, and the plots of I_0/I vs. [Q] are depicted in Fig. 4. The figure obviously demonstrates that incremental addition of metal complex concentration causes the decrease in fluorescence intensity. It may suggest that EB molecules are replaced by the metal complexes at their DNA binding sites [35]. Fluorescence quenching study in the presence of the complex has been analyzed further by Stern–Volmer equation as follows [36],

$$I_0/I = K_{SV}[Q] + 1 \quad (1)$$

where I_0 and I are the fluorescence intensities in the absence and presence of quencher (metal complexes), respectively; [Q] is the concentration of the quencher and K_{SV} is the Stern–Volmer quenching constant (slope of plot between I_0/I and [Q]). The obtained values of Ksv for the metal complexes are $4.81 \times 10^4\ M^{-1}$ and $2.48 \times 10^4\ M^{-1}$, respectively and they propose the intercalative binding of metal complexes with DNA.

Table 1 Change in electronic absorption parameters for the complexes on interaction with CT DNA in 5 mM Tris HCl/50 mM NaCl buffer (pH 7.2)

Compound	λ max		Δλ (nm)	H%	$K_b \times 10^5\ (M^{-1})$
	Free	Bound			
$[CuL(His)_2]$	380.6	379.4	1.2	10.4	5.8
$[CoL(His)_2]$	381.1	379.3	2.2	6.3	1.4
$[NiL(His)_2]$	377.2	376.1	1.1	7.5	2.8
$[ZnL(His)_2]$	380.2	379.1	1.1	7.1	3.7

$H\% = [(A_{free} - A_{bound})/A_{free}] \times 100\ \%$; K_b = intrinsic binding constant

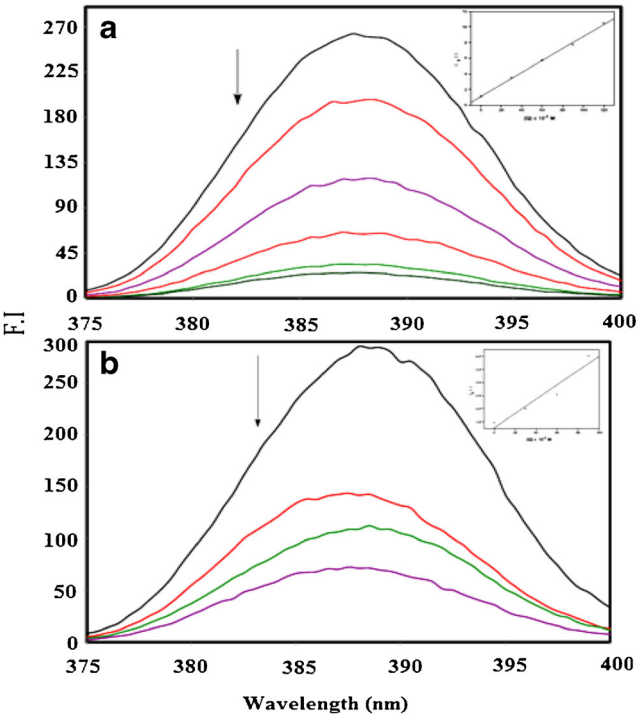

Fig. 4 Fluorescence quenching curves of EB bound to DNA: **a** $[CuL(His)_2]$ and **b** $[ZnL(His)_2]$ [DNA] = 10 μL, [EB] = 5 μL, [Complex] = 0–120 μL. (Inset: Plot of I_0/I vs [Q])

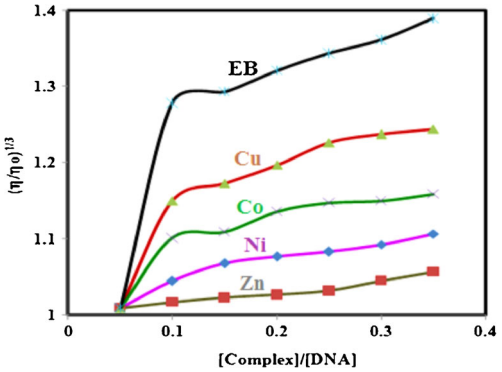

Fig. 5 Effect of increasing amounts of [EB] (*), $[CuL(His)_2]$ (▲), $[CoL(His)_2]$ (×)], $[NiL(His)_2]$ (♦) and $[ZnL(His)_2]$ (■) on the relative viscosity of CT DNA. Plot of relative viscosity $(\eta/\eta o)^{1/3}$ vs [Complex]/[DNA]

Viscosity Measurement

The DNA binding has been further investigated by viscosity studies. In significant, viscosity measurements can afford strong support in favor of intercalative binding. The intercalative binding is very sensitive to the changes in the length of the DNA molecule. Viscosity measurements are considered as the least ambiguous and they are effective in determining the changes in length of DNA and thus deciding the binding mode of metal complexes with DNA in solution [37]. In this work, viscosity analysis was carried out on DNA solutions by increasing the amount of the complexes. In classical intercalation, base pairs of DNA are separated to accommodate metal complexes in between them (intercalation sites) as a result the viscosity of DNA gets strengthened [38]. With this background, the analyzed relative specific viscosities of DNA both in the absence and presence of the complex are plotted against [complex]/[DNA] as shown in Fig. 5. It is observed that the addition of the complex to CT DNA solution leads to an increase in the viscosity of CT DNA, thereby intercalative mode of binding between metal complex and CT DNA is confirmed.

Electrochemical Titration

Likewise the above studies, CV and difference pulse voltammetry (DPV) are also widely employed techniques to probe the binding mode of metal complexes with DNA. CV and DPV methods are considered to be the sensitive analytical instruments to determine the changes in oxidation state of the metallic species in the presence of biomolecules. In the present cram, CV and DPV have been applied to find out the nature of DNA binding mode [39]. The cyclic voltammograms of $[CuL(His)_2]$, $[CoL(His)_2]$, $[NiL(His)_2]$ and $[ZnL(His)_2]$ have been collected both in absence and presence of DNA. The effect of increase of DNA concentration on cyclic voltammograms of the studied complexes is presented in Fig. 6. Incremental addition of DNA effectively alters both potentials and currents of anodic as well cathodic peaks. This affirms the interaction existing between the complex and DNA [40].

The parameters received from CV study of complexes both in presence and absence of DNA are given in Table 2. In the absence of DNA, CV of $[CuL(His)_2]$ reveals four characteristic peaks in which two are anodic, E_{pa} (−0.409 and −0.034 V) and two are cathodic, E_{pc} (−0.684 and −1.233 V). From the two separate anodic and cathodic peaks, two redox couples are assumed as follows:

$$\mathrm{Cu(II)}\rightarrow\mathrm{Cu(I)}\left(\mathrm{Epa}=-0.409\ \mathrm{V};\mathrm{Epc}=-0.684\ \mathrm{V};\ \Delta\mathrm{Ep}=0.275\ \mathrm{V}\ \text{and}\ \mathrm{E1/2}=-0.546\ \mathrm{V}\right);$$
$$\mathrm{Cu(I)}\rightarrow\mathrm{Cu(0)}\left(\mathrm{Epa}=-0.034\ \mathrm{V};\mathrm{Epc}=-1.233\ \mathrm{V};\ \Delta\mathrm{Ep}=1.199\ \mathrm{V}\ \text{and}\ \mathrm{E}_{1/2}=-0.633\ \mathrm{V}\right).$$

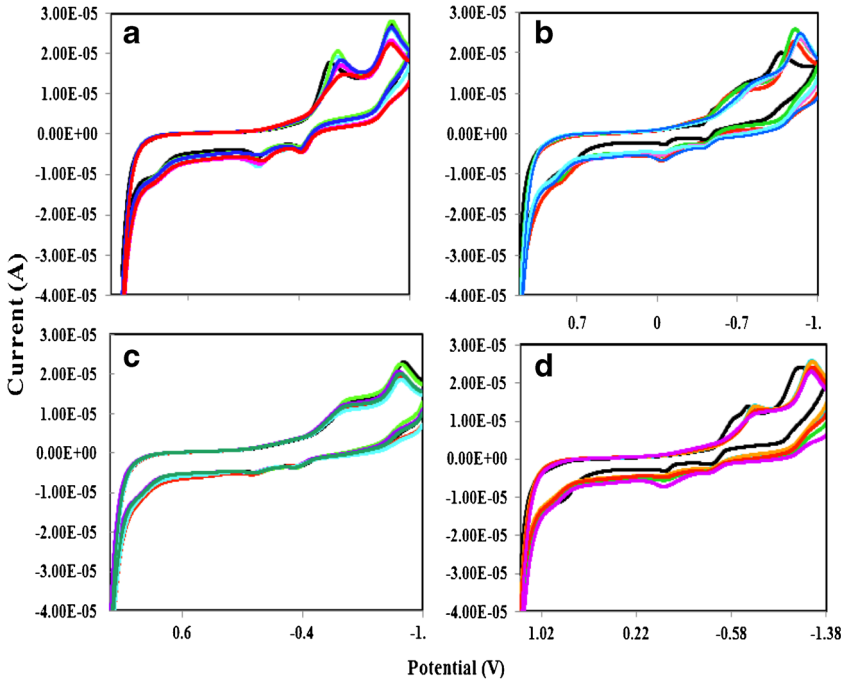

Fig. 6 Cyclic voltammograms of **a** $[CuL(His)_2]$, **b** $[CoL(His)_2]$, **c** $[NiL(His)_2]$ and **d** $[ZnL(His)_2]$ in buffer (pH = 7.2) at 25 °C in presence of increasing amount of DNA

$[CoL(His)_2]$ shows only one redox couple in the absence of DNA and its details are given below:

$$Co(II)\rightarrow Co(I),\ (Epa = -0.418\ V,\ Epc = -1.081\ V,\ \Delta Ep = -0.663\ V,\ \text{and}\ E_{1/2} = -0.749\ V).$$

Likewise $[NiL(His)_2]$ shows one redox couple in the absence of DNA and it is detailed below:

$$Ni(II)\rightarrow Ni(I),\ (Epa = -0.351\ V,\ Epc = -1.217\ V,\ \Delta Ep = 0.866\ V,\ \text{and}\ E_{1/2} = -0.784\ V).$$

CV study of $[ZnL(His)_2]$ in the absence of DNA results in only one redox couple and the details are provided below:

$$Zn(II)\rightarrow Zn(0),\ (Epa = -0.011\ V,\ Epc = -1.204\ V,\ \Delta Ep = 1.193\ V,\ \text{and}\ E_{1/2} = -0.607\ V).$$

Irrespective of the complexes, all the above redox couples are found to have approximately unity peak current ratio which recommends that they are quasi-reversible redox processes.

DPV of all the complexes both in the absence and presence of DNA are depicted in supplementary file (Fig. S4). The changes in potential as well as current density during the incremental addition of DNA to the complex solution confirm the intercalative mode of interactions. The synthesized complexes give both the anodic and cathodic peak potential shifts upon the addition of DNA. These shifts specify the intercalating mode of DNA binding with complexes [29, 41].

DNA Cleavage

DNA cleavage ability of the synthesized complexes was investigated by gel electrophoresis on super coiled plasmid pUC19 DNA in the medium of Tris–acetate–EDTA (TAE) buffer solution. Prior to the experiments, the reaction mixture was incubated under physiological conditions for 1 h. The previous report explains that when super coiled form (Form I) of plasmid pUC19 DNA is nicked, an open circular relaxed form (Form II) is formed and the linear form (Form III) is found upon further cleavage [42]. During electrophoresis of reaction mixture in the presence of activating agent (H_2O_2), in general, relatively a fast migration will be observed for the

Table 2 Redox potential profiles for interaction of DNA with metal complexes

Compound	$E_{1/2}(V)^a$		$^b\Delta Ep(V)$		Ip_a/Ip_c	$K[red]/K[oxd]$
	Free	Bound	Free	Bound		
$[CuL(His)_2]$	−0.546 −0.633	−0.805 −0.543	0.275 1.199	0.882 0.734	0.62	0.287
$[CoL(His)_2]$	−0.749	−0.632	0.663	0.491	0.98	0.732
$[NiL(His)_2]$	−0.784	−0.543	0.866	0.452	0.94	0.857
$[ZnL(His)_2]$	−0.607	−0.578	1.193	0.476	0.96	0.219

Data from cyclic voltammetric measurements: $^a E_{1/2}$ is calculated as the average of anodic (E_{Pa}) and cathodic (E_{pc}) peak potentials; $E_{1/2}{}^a = E_{Pa} + E_{pc}/2$; $^b \Delta Ep = E_{pa} - E_{pc}$

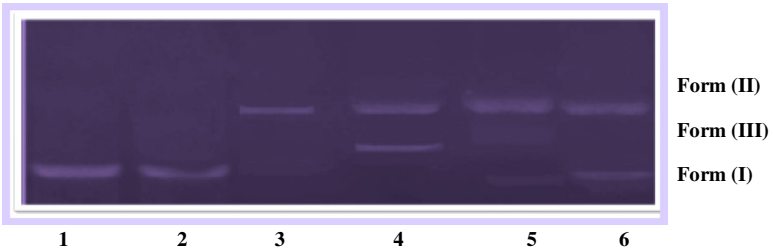

Fig. 7 Gel electrophoresis diagram showing the cleavage of pUC19 DNA (10 μM) by the complexes in Tris–acetate–EDTA (TAE) buffer in presence of hydrogen peroxide : Lane 1, DNA; Lane 2, DNA + L + H_2O_2; Lane 3, DNA + [$CuL(His)_2$] + H_2O_2; Lane 4, DNA + [$CoL(His)_2$] + H_2O_2; Lane 5, DNA + [$NiL(His)_2$] + H_2O_2; Lane 6, DNA + [Zn $L(His)_2$] + H_2O_2

intact supercoiled form (Form I). If scission occurs on one strand, the super coil will relax to generate a slower moving open circular form (Form II). If both the strands are cleaved, a linear form (Form III) that migrates in between Form I and II will be generated [43]. As seen from Fig. 7, the control experiments with DNA alone (lane 1) and DNA presence of L (lane 2) do not show any cleavage activity. But the complexes convert super coiled DNA (Form I) into nicked circular DNA (Form II) with admirable DNA cleaving properties. These observations assert that a combination of studied complexes and H_2O_2 are very essential to show effectual cleavage of DNA. This damage may be attributed to the formation of hydroxyl free radicals. The OH free radicals participate in the oxidation of the deoxyribose moiety, followed by hydrolytic cleavage of a sugar phosphate back bone. The DNA cleavage facility of the metal complexes may also depend on the extensive binding of the DNA molecules to the metal complexes [44]. It may also be concluded that complexes which cleave the DNA may also inhibit the growth of the pathogenic organism by cleaving the genome.

Antimicrobial Screening

Owing to the greatest involvement of antimicrobial screening in the medicine and pharmaceutical fields, it has been done with L and the complexes. The minimum inhibitory concentration (MIC) values of measured in antibacterial and antifungal studies of the complexes are given in Tables 3 and 4. It is observed that L functions ineffectively against the chosen bacteria and fungi as compared to the complexes. Such better activity of complexes over L can be explained by Overtone's concept and Tweedy's chelation theory [45]. The presence of imine (−C=N) group in the structure of the complexes would enhance their activity due to the chelating effect which makes them as more powerful antibacterial agents and thereby killing the microbe or inhibiting multiplication of the microbe via blocking their active sites [46]. In the mechanistic approach, chelation considerably reduces the polarity of the metal ion because of partial sharing of its positive charge with donor groups and possible electron delocalization over the whole chelate ring. It could enhance the lipophilic character of the central metal atom, which subsequently favours its permeation through the lipid layer of the cell membrane. Eventually the complexes block all the metal binding sites in the enzymes of microorganisms. The complexes also disturb the respiration process and thus block the synthesis of the proteins which restricts further growth of the organisms. It is found that the presence of electron withdrawing groups such as *methoxy* group in the complexes reveals a comparable growth-inhibitory activity against microorganisms. The presence of such electron withdrawing in the present complexes would further add the attraction to their biological properties.

Molecular Docking Study

Molecular docking technique is an attractive scaffold to understand the drug- nucleic acid interactions for the development of modern drug design and to confirm the exact binding site available at the molecular target DNA particularly in a non-covalent fashion [47].

Molecular docking studies on L and metal complexes have been carried out with DNA duplex of sequence *d*(CGCGAA TTCGCG)$_2$ dodecamer (PDB ID: 1BNA). In this study L and complexes have been successively docked with DNA to predict the appropriate binding site and preferred orientation of the molecules inside DNA. It is generally accepted that the lower the binding free energy, the more potent the binding affinity is between the receptor (DNA) and "the ligand" (Schiff base and its metal complexes) molecules. Thus the

Table 3 Minimum inhibitory concentration of the synthesized hybrids against the growth of bacteria (μM)

Compound	Minimum inhibitory concentration (MIC) ($\times 10^4$ μM)			
	S. aurous	*N.asteroides*	*K. pneumoniae*	*E. coli*
[L]	15.2	15.9	17.5	16.8
[$CuL(His)_2$]	5.6	5.4	6.3	6.2
[$CoL(His)_2$]	7.3	8.1	9.2	9.5
[$NiL(His)_2$]	7.1	7.4	8.2	8.4
[$ZnL(His)_2$]	9.1	8.9	9.4	10.3
Ciprofloxacin	3.1	3.4	3.9	4.1

Table 4 Minimum inhibitory concentration of the synthesized hybrids against the growth of fungi (μM)

Compound	Minimum inhibitory concentration (MIC) ($\times 10^4$ μM)		
	A. niger	*F.solani*	*C.albicans*
[L]	19.7	17.1	18.8
$[CuL(met)_2]$	7.5	6.9	5.8
$[CoL(met)_2]$	7.9	6.2	8.2
$[NiL(met)_2]$	10.2	9.5	8.7
$[ZnL(met)_2]$	12.2	11.3	10.2
Fluconazole	3.2	2.9	2.4

molecular docking calculations were performed and the most probable docked poses are depicted in Fig. 8. This figure clearly shows that the L and complexes interact with DNA via an intercalation mode involving outside edge stacking interaction with oxygen atom of the phosphate backbone. As seen from Fig. 8, it is clear that the ligand and complexes fit well into the intercalation mode of targeted DNA [48]. Further, resulting structures are stabilized by van der Waals interaction and hydrophobic contacts with DNA functional group that define the stability of intercalations [49]. The resulting binding energy of docked L and metal complexes were found to be −225.98 (L) and −284.78 (Cu), −284.64 (Co), −283.89 (Ni) and −284.64 (Zn) KJ mol^{-1} respectively. Hence, it shows that the observed binding energy score of the present complexes is higher than that of a few metal complexes available in the literature [11]. The more negative the relative binding energy, greater the binding of the complex with DNA, which is consistent with the DNA binding affinity obtained from in vitro DNA binding experimental studies and indicated greater binding affinity of complexes is more prominent DNA binder than ligand. Thus, we can conclude that there is a mutual complement between spectroscopic techniques and molecular docked model, which can be substantiate our spectroscopic results and at the same time provides further evidence of intercalation mode.

Conclusion

A novel and innovative hetrocylic imine ligand which is capable of making chelating complexes with improved biological properties has been synthesized and characterized. Four metal (Cu(II), Co(II), Ni(II) and Zn(II)) complexes have been synthesized from L and characterized by physicochemical,

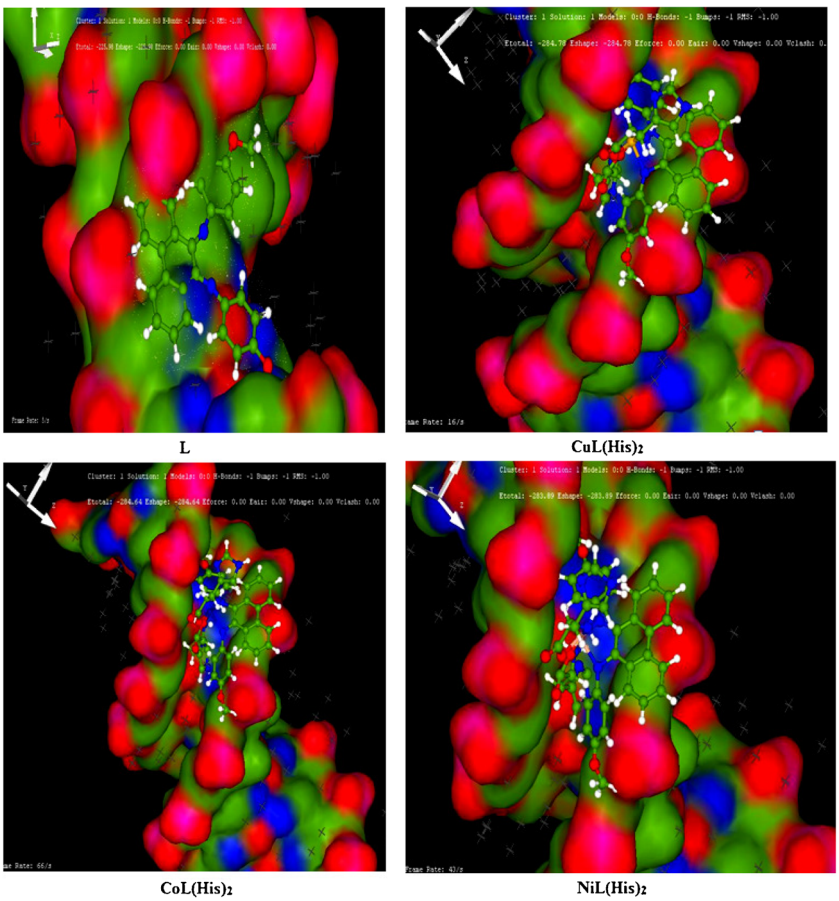

Fig. 8 Molecular docked model of L and its complexes with DNA

spectral and electrochemical techniques. The role of amino acid as a co-ligand would hopefully take the studied compelxes as more bio-relevant. All the complexes have octahedral geometry except Cu(II) complex which has the same with distortion. The interaction of the complexes with DNA has been effectively examined and explored by fluorescence titration, UV–Vis., absorption, viscometer titration, cyclic voltammetry (CV), differential pulse voltammetry and molecular docking analysis. These studies prove that CT DNA interaction of the complexes follows intercalation mode. The DNA cleavage activity of all the metal complexes with pUC19 DNA under aerobic conditions is efficient cleavage in the presence of oxidizing agent (H_2O_2). The antimicrobial screening indicates that these complexes are good antimicrobial agents against various organisms and standards. These experiments assume consequence as they provide the mode of the complex binding to DNA and the complexes act as specific targets for the rational design of DNA structure probes.

Acknowledgments The authors express their heartfelt thanks to the College Managing Board, Principal, and Head of the Department of Chemistry, VHNSN College for providing necessary research facilities to complete this work successfully. The characterization facilities afforded by IIT Bombay and CDRI, Lucknow are gratefully acknowledged by all authors.

References

1. Yang W, Liu H, Du D (2010) Efficient in situ three-component formation of chiral oxazoline-Schiff base copper(II) complexes: towards combinatorial library of chiral catalysts for asymmetric Henry reaction. Org Biomol Chem 8:2956–2960
2. Krishnamoorthy P, Sathyadevi P, Muthiah PT, Dharmaraj N (2012) Nickel and cobalt complexes of benzoic acid (2-hydroxybenzylidene)-hydrazide ligand: synthesis, structure and comparative in vitro evaluations of biological perspectives. RSC Adv 2: 12190–12203
3. Lukmantara AY, Kalinowski DS, Kumar N, Richardson DR (2014) Synthesis and biological evaluation of 2-benzoylpyridine thiosemicarbazones in a dimeric system: structure-activity relationship studies on their anti-proliferative and iron chelation efficacy. J Inorg Biochem 141:43–54
4. Lahiri D, Majumdar R, Mallick D, Goswami TK, Dighe RR, Chakravarty AR (2011) Remarkable photocytotoxicity in hypoxic HeLa cells by a dipyridophenazine copper(II) Schiff base thiolate. J Inorg Biochem 105:1086–1094
5. Arjmand F, Parveen S (2012) Enantiomeric recognition of chiral L– and D–penicillamine zinc(II) complexes: DNA binding behavior and cleavage studies. RSC Adv 2:6354–6362
6. Antony R, Manickam STD, Kollu P, Chandrasekar PV, Karuppasamy K, Balakumar S (2014a) Highly dispersed Cu(II), Co(II) and Ni(II) catalysts covalently immobilized on imine-modified silica for cyclohexane oxidation with hydrogen peroxide. RSC Adv 4:24820–24830
7. Ghiaci M, Rezaei B, Arshadi M (2009) Characterization of modified carbon paste electrode by using salen Schiff base ligand immobilized on SiO2–Al2O3 as a highly sensitive sensor for anodic stripping voltammetric determination of copper(II). Sensors Actuators B 139:494–500
8. Mrkalić E, Zianna A, Psomas G, Gdaniec M, Czapik A, Argyropoulou EC, Kantouri ML (2014) Synthesis, characterization, thermal and DNA-binding properties of new zinc complexes with 2-hydroxyphenones. J Inorg Biochem 134:66–75
9. Mendu P, Kumari CG, Ragi R (2015) Synthesis, characterization, DNA binding, DNA cleavage and antimicrobial studies of Schiff base ligand and its metal complexes. J Fluoresc 25:369–378
10. Shamsi M, Yadav S, Arjmand F (2014) Synthesis and characterization of new transition metal {Cu(II), Ni(II) and Co(II)} L-phenylalanine-DACH conjugate complexes: in vitro DNA binding, cleavage and molecular docking studies. J Photochem Photobiol B 136:1–11
11. Lauria A, Bonsignore R, Terenzi A, Spinello A, Giannici F, Longo A, Almerico AM, Barone G (2014) Nickel(II), copper(II) and zinc(II) metallo-intercalators: structural details of the DNA-binding by a combined experimental and computational investigation. Dalton Trans 43:108–6119
12. Deschamps P, Kulkarni PP, Basak MG, Sarkar B (2005) The saga of copper(II)–L-histidine. Coord Chem Rev 249:895–909
13. Kawahara M, Sadakane Y, Koyama H, Konoha K, Ohkawara S (2013) D-histidine and L-histidine attenuate zinc-induced neuronal death in GT1-7 cells. Metallomics 5:453–460
14. Dehghan G, Dolatabadi JEN, Jouyban A, Zeynali KA, Ahmadi SM, Kashanian S (2010) Spectroscopic studies on the interaction of quercetin–terbium(III) complex with calf thymus DNA. DNA Cell Biol 30:95–201
15. Anbu S, Shanmugaraju S, Kandaswamy M (2012) Electrochemical, phosphate hydrolysis, DNA binding and DNA cleavage properties of new polyaza macrobicyclic dinickel(II) complexes. RSC Adv 2:5349–5357
16. Lerman LS (1961) Structural considerations in the interaction of DNA and acridines. J Mol Biol 3:18–14
17. Zheng K, Liu F, Xu XM, Li YT, Wu ZY, Yan CW (2014) Synthesis, structure and molecular docking studies of dicopper(II) complexes bridged by N-phenolato-N′-[2-(dimethylamino)ethyl]oxamide: the influence of terminal ligands on cytotoxicity and reactivity towards DNA and protein BSA. New J Chem 38:2964–2978
18. Ganeshpandian M, Ramakrishnan S, Palaniandavar M, Suresh E, Riyasdeen A, Akbarsha MA (2014) Mixed ligand copper(II) complexes of 2,9-dimethyl-1,10- phenanthroline: tridentate 3 N primary ligands determine DNA binding and cleavage and cytotoxicity. J Inorg Biochem 140:202–212
19. Antony R, Manickam STD, Karuppasamy K, Kollu P, Chandrasekar PV, Balakumar S (2014b) Organic–inorganic hybrid catalysts containing new Schiff base for environment friendly cyclohexane oxidation. RSC Adv 4:42816–42824
20. Barwiolek M, Szlyk E, Berg A, Wojtczak A, Muziol T, Jezierska J (2014) Structural studies of copper(II) complexes with 2-(2-aminoethyl)pyridine derived Schiff bases and application as precursors of thin organic–inorganic layers. Dalton Trans 2:9924–9933
21. Chew ST, Lo KM, Sinniah SK, Sim KS, Tan KW (2014) Synthesis, characterization and biological evaluation of cationic hydrazone copper complexes with diverse diimine co-ligands. RSC Adv 4: 61232–61247
22. Kumar RS, Arunachalam S (2007) DNA binding and antimicrobial studies of some polyethyleneimine-copper(II) complex samples containg 1,10-phenanthroline and 1-theroline as co-ligands. Polyhedron 26:3255–3262
23. Dhanaraj CJ, Johnson J (2014) Synthesis, characterization, electrochemical and biological studies on some metal(II) Schiff base complexes containing quinoxaline moiety. Spectrochim Acta 118:624–631
24. Haghighi FH, Hadadzadeh H, Darabi F, Jannesari Z, Ebrahimi M, Khayamian T, Salimi M, Rudbari HA (2013) Polypyridyl Ni(II)

complex, [Ni(tppz)2]2+: structure, DNA and BSA binding and molecular modeling. Polyhedron 65:16–30
25. Tabassum S, Zaki M, Arjmand F, Ahmad I (2012) Synthesis, characterization and interaction studies of copper based drug with human serum albumin (HSA): spectroscopic and molecular docking investigations. J Photochem Photobiol B 114:108–118
26. Estermann M, David W (2002) Structure determination from powder diffraction data. Oxford
27. Silva AR, Freitas MMA, Freire C, Castro BD, Figueiredo JL (2002) Heterogenization of a functionalized copper(II) Schiff base complex by direct immobilization onto an oxidized activated carbon. Langmuir 18:8017–8024
28. Bew MJ, Hathaway BJ, Fereday RJ (1972) Electronic properties and stereochemistry of the copper(II) ion. Part VII. Mono(diethylenetriamine)copper(II) complexes. Dalton Trans 12: 1229–1237
29. Hathaway BJ, Billing DE (1970) The electronic properties and stereochemistry of mono-nuclear complexes of the copper(II) ion. Coord Chem Rev 5:143–207
30. Raja DS, Bhuvanesh NSP, Natarajan K (2012) A novel water soluble ligand bridged cobalt(II) coordination polymer of 2-oxo-1,2-dihydroquinoline-3-carbaldehyde (isonicotinic) hydrazone: evaluation of the DNA binding, protein interaction, radical scavenging and anticancer activity. Dalton Trans 41:4365–4377
31. Zhou CY, Zhao J, Wu YB, Yin CX, Pin Y (2007) Synthesis, characterization and studies on DNA-binding of a new Cu(II) complex with N1,N8-bis(1-methyl-4-nitropyrrole-2-carbonyl)triethylenetetramine. J Inorg Biochem 101:10–18
32. Li L, Guo Q, Dong J, Xu T, Li J (2013) DNA binding, DNA cleavage and BSA interaction of a mixed-ligand copper(II) complex with taurine Schiff base and 1,10-phenanthroline. J Photochem Photobiol B 125:56–62
33. Li P, Niu M, Hong M, Cheng S, Dou J (2014) Effect of structure and composition of nickel(II) complexes with salicylidene Schiff base ligands on their DNA/protein interaction and cytotoxicity. J Inorg Biochem 137:101–108
34. Rajarajeswari C, Loganathan R, Palaniandavar M, Suresh E, Riyasdeen A, Akbarsha MA (2013) Copper(II) complexes with 2NO and 3N donor ligands: synthesis, structures and chemical nuclease and anticancer activities. Dalton Trans 42:8347–8363
35. Paul A, Gupta RK, Dubey M, Sharma G, Koch B, Hundal G, Hundal MS, Pandey DS (2014) Potential apoptosis inducing agents based on a new benzimidazole schiff base ligand and its dicopper(II) complex. RSC Adv 4:41228–41236
36. Biver T, Secco F, Tine MR, Venturini M (2004) Kinetics and equilibria for the formation of a new DNA metalintercalator: the cyclic polyamine neotrien/copper(II) complex. J Inorg Biochem 98:33–40
37. Tolia GPC, Papadopoulos AN, Raptopoulou CP, Psycharis V, Garino C, Salassa L (2013) Copper(II) interacting with the non-steroidal antiinflammatory drug flufenamic acid: structure, antioxidant activity and binding to DNA and albumins. J Inorg Biochem 123:53–65
38. Prabahara MC, Naik HSB (2008) Binding and photocleavage of DNA by mixed ligand Co(III) and Ni(II) complexes of thiophene[2, 3-b]quinoline and phenanthrolie/bipyridine. Biometals 21:675–684
39. Bard AJ, Faulkner LR (1980) Electrochemical methods: fundamentals and applications. Wiley, New York
40. Carter MT, Bard AJ (1987) Voltammetric studies of the interaction of tris(1,10 phenanthroline) cobalt(III) with DNA. J Am Chem Soc 109:7528–7530
41. Blackburn GM, Gait MJ (1996) Nucleic acid in chemistry and biology. Oxford University Press, New York
42. Brissos RF, Torrents E, Mello FMDS, Pires WC, Lacerda EPS, Caballero AB, Caubet A, Massera C, Roubeau O, Teat SJ, Gamez P (2014) Highly cytotoxic DNA-interacting copper(II) coordination compounds. Metallomics 6:1853–1868
43. Tabassum S, Afzal M, Arjmand F (2014) New modulated design, docking and synthesis of carbohydrate-conjugate heterobimetallic Cu(II), Sn(II) complex as potential topoisomerase II inhibitor: in vitro DNA binding, cleavage and cytotoxicity against human cancer cell lines. Eur J Med Chem 74:694–702
44. Kashanian S, Ezzati J, Dolatabadi N (2009) In vitro study of calf thymus DNA interaction with butylated hydroxyanisole. DNA Cell Biol 28:535–540
45. Priya P, Arunachalam SV, Sathya N, Chinnusamy V, Jayabalakrishnan C (2009) Catalytic and antimicrobial studies of binuclear ruthenium(III) complexes containing bis-β-diketones. Transit Met Chem 34:437–442
46. Ramesh R, Maheswaran S (2003) Synthesis, spectra, dioxygen affinity and antifungal activity of Ru(III) Schiff base complexes. J Inorg Biochem 96:457–462
47. Lakshmipraba J, Arunachalam S, Solomon RV, Venuvanalingam P, Riyasdeenb A, Dhivyac R, Akbarshab MA (2015) Surfactant–copper(II) Schiff base complexes: synthesis, structural investigation, DNA interaction, docking studies, and cytotoxic activity. J Biomol Struct Dyn 33:877–891
48. Barone G, Terenzi A, Lauria A, Almerico AM, Leal JM, Busto L, García B (2013) DNA-binding of nickel(II), copper(II) and zinc(II) complexes: structure–affinity relationships. Coord Chem Rev 257: 2848–2862
49. Tabassum S, Zaki M, Arjmand F (2013) New modulated design and synthesis of quercetin– Cu^{II}/Zn^{II}–$Sn2^{IV}$ scaffold as anticancer agents: in vitro DNA binding profile, DNA cleavage pathway and -I activity. Dalton Trans 42:10029–10041